IEEE Photonics Journal
An IEEE Photonics Society Publication

Open Access

GHz Optical Time-Stretch Microscopy by Compressive Sensing

Volume 9, Number 2, April 2017

Cheng Lei
Yi Wu
Aswin C. Sankaranarayanan
Shih-Min Chang
Baoshan Guo
Naoto Sasaki
Hirofumi Kobayashi
Chia-Wei Sun
Yasuyuki Ozeki, *Member, IEEE*
Keisuke Goda, *Senior Member, IEEE*

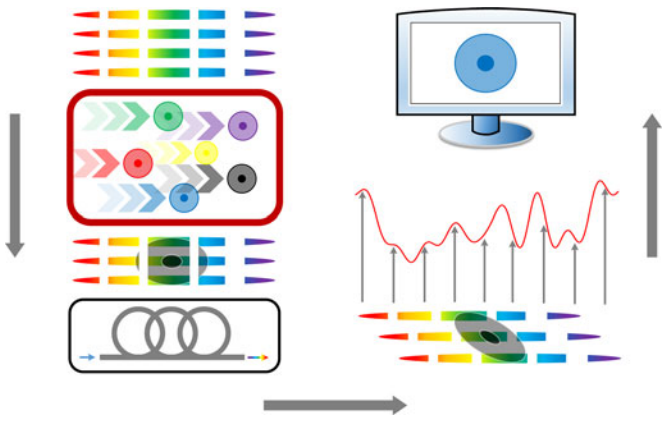

DOI: 10.1109/JPHOT.2017.2676349

IEEE photonics SOCIETY

IEEE

GHz Optical Time-Stretch Microscopy by Compressive Sensing

Cheng Lei,[1,2] Yi Wu,[1,3] Aswin C. Sankaranarayanan,[4] Shih-Min Chang,[1,5] Baoshan Guo,[1] Naoto Sasaki,[1] Hirofumi Kobayashi,[1] Chia-Wei Sun,[5] Yasuyuki Ozeki,[6] *Member, IEEE*, and Keisuke Goda,[1,7,8] *Senior Member, IEEE*

[1]Department of Chemistry, University of Tokyo, Tokyo 113-0033, Japan
[2]Department of Electronic Engineering, Tsinghua University, Beijing 100084, China
[3]Department of Materials Science and Engineering, Carnegie Mellon University, Pittsburgh, PA 15213 USA
[4]Department of Electrical and Computer Engineering, Carnegie Mellon University, Pittsburgh, PA 15213 USA
[5]Department of Photonics, National Chiao Tung University, Hsinchu 30010, Taiwan
[6]Department of Electrical Engineering and Information Systems, University of Tokyo, Tokyo 113-8656, Japan
[7]Japan Science and Technology Agency, Kawaguchi 332-0012, Japan
[8]Department of Electrical Engineering, University of California, Los Angeles, CA 90095 USA

DOI:10.1109/JPHOT.2017.2676349

Manuscript received January 21, 2017; revised February 23, 2017; accepted February 24, 2017. Date of publication March 1, 2017; date of current version March 17, 2017. This work was primarily supported by the ImPACT Program of the Cabinet Office, Government of Japan (CSTI) and in part by Noguchi Shitagau Research Grant, in part by the New Technology Development Foundation, in part by Konica Minolta Imaging Science, in part by JSPS KAKENHI under Grant 25702024 and Grant 25560190, in part by JGC-S Scholarship Foundation, in part by Mitsubishi Foundation, in part by the TOBIRA Award, and in part by the Takeda Science Foundation. The work of C. L. and K. G. was supported in part by the International Postdoctoral Exchange Fellowship Program 2014 of the Office of the China Postdoctoral Council and Burroughs Wellcome Foundation, respectively. Corresponding author: C. Lei (E-mail: leicheng@chem.s.u-tokyo.ac.jp).

Abstract: Optical time-stretch microscopy has recently attracted intensive attention for its capability of acquiring images at an ultrahigh frame rate. Unfortunately, its achievable frame rate is limited by the requirement of having no overlap between consecutive frames, which leads to a tradeoff between the frame rate (pulse repetition rate) and the amount of the temporal dispersion used for optical image serialization. In this paper, we demonstrate compressive sensing on the platform of optical time-stretch microscopy to overcome the tradeoff between frame rate and temporal dispersion (time stretch) and achieve 50 times higher frame rate than conventional optical time-stretch microscopy. Specifically, we computationally perform compressed optical time-stretch microscopy with an experimental dataset acquired by conventional optical time-stretch microscopy and demonstrate its effects in terms of spatial resolution and cell classification accuracy. Our results indicate that the spatial resolution and cell classification accuracy reach 780 nm and 95% at a line scan rate of 675 MHz and 6.75 GHz, respectively, which correspond to five times and 50 times higher frame rates than what conventional optical time-stretch microscopy can achieve with the same dispersion amount and digitizer sampling rate.

Index Terms: Compressive sensing (CS), time-stretch microscopy, image processing.

1. Introduction

Over the past decade, breathtaking innovations in optical microscopy have been witnessed in diverse fields. Such innovations include optical coherence tomography [1], super-resolved fluorescence microscopy [2], lensless microscopy [3], and optical time-stretch microscopy [4]–[7]. Optical time-stretch microscopy is a technique that enables ultrafast multi-dimensional image acquisition by illuminating the object with a spectrally structured laser pulse, optically stretching or serializing every image frame into a 1-D time-domain waveform with temporal dispersion, detecting and digitizing the waveform with a single-pixel photodetector and single digitization channel, and reconstructing the image frame digitally. By virtue of its capability to acquire images at an ultrahigh frame rate of higher than 10 Mfps, optical time-stretch microscopy has been proven useful for many applications such as surface inspection, particle analysis, and cell screening.

Unfortunately, the maximum possible frame rate of optical time-stretch microscopy is limited by its requirement of having no overlap between consecutive frames or, more specifically, a trade-off between the frame rate (pulse repetition rate) and the amount of the temporal dispersion (time stretch) used for the optical image serialization [4], [6]. In optical time-stretch microscopy, each image-encoded pulse is temporally stretched by a temporal disperser into a temporal waveform that fills the gap between consecutive image-encoded pulses (frames). Ideally, the frame rate of the system can easily be increased by applying a pulse laser with a higher repetition rate. However, to ensure the information carried on the pulses to be perfectly recovered, there should be no overlap between temporally stretched pulses. Given a fixed sampling rate for the digitizer, a certain amount of temporal dispersion is required for a desirable number of sampled points or image pixels. This limits the maximum repetition rate of the pulse laser and hence the frame rate of the system. Analytically, given the pulse bandwidth $\Delta\lambda$, the digitizer sampling rate S, and the desired number of sampling points for each pulse N, the minimum dispersion amount required is given by $D = N/(S\Delta\lambda)$. This places an upper limit for the applicable laser repetition rate R by $R < S/N$ in order to avoid an overlap between temporally stretched pulses [4], [6]. Consequently, to increase the frame rate of the system, it is necessary to further increase the upper limit of the laser repetition rate. To avoid degradation of the image quality (hence to maintain the same number of sampling points for each pulse), a digitizer with a higher sampling rate is typically needed. This, however, significantly increases the cost of the overall system and also comes with the massive volume of data to be processed.

In this paper, we overcome this trade-off by using compressive sensing (random spatial coding) [8], [9] into laser pulses (frames) and recovering the spatial profile of the object, even with a significant frame overlap of more than 98% (in frame area) between the consecutive frames. Hence, a pulse laser with a much higher repetition rate can be used to achieve 50 times higher frame rate than conventional optical time-stretch microscopy with the same dispersion amount and digitizer sampling rate. To validate the capability of this method, we computationally perform compressed optical time-stretch microscopy with an experimental dataset acquired by a conventional optical time-stretch microscope and evaluate recovered images with the modulation transfer function (MTF) and structural similarity (SSIM) index, which are routinely used for evaluating the resolution of an optical imaging system [10] and predicting the perceived quality of digital images and measuring the similarity between two digital images [11], respectively. Furthermore, we also computationally perform compressed optofluidic time-stretch microscopy on the images of microalgal cells (*Euglena gracilis*) flowing in a microfluidic device and evaluate it in terms of cell classification accuracy. Our results indicate that the spatial resolution and cell classification accuracy reach 780 nm and 95% at a line scan rate of 675 MHz and 6.75 GHz, respectively, which correspond to five times and 50 times higher frame rates than conventional optical time-stretch microscopy with the same dispersion amount and digitizer sampling rate.

2. Principles

Our compressed optical time-stretch microscope is schematically shown in Fig. 1. A pulse laser is employed as the optical source. The pulses are first spatially dispersed by a diffraction grating, and

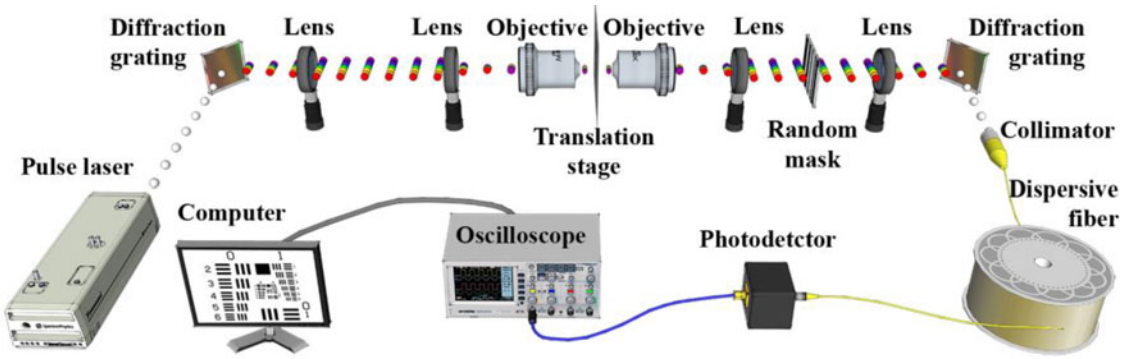

Fig. 1. Schematic of compressed optical time-stretch microscopy.

then focused onto the target object by an objective lens. As a result, the 1-D cross-sectional profiles of the object in the lateral direction (perpendicular to the movement) are encoded on the spectra of the incoming pulses. The transmitted pulses through the object are collected by a second objective lens, modulated by a random binary mask, and recombined by a second diffraction grating. After that, the pulses are coupled into the temporal disperser, which is a fiber spool here, and stretched in the time domain. Pulses are repeated while the object is also moving or flowing. If the gap between the consecutive pulses is shorter than the temporal broadening, which is the situation of this compressed optical time-stretch microscopy, the pulses significantly overlap with their neighboring pulses. Finally, the overlapped pulses are detected by a photodetector and digitized by a digitizer. Since each pulse is randomly modulated in the spatial domain and relatively shifted in the time domain due to their different arrival times, the 2-D profile of the object whose 1-D sections are encoded in the pulses can be recovered by employing convex optimization algorithms. In theory, the spatial modulation of the pulses with the binary random mask can be implemented either before or after the image-encoding part, but if the spatial size of the random pattern is under the resolution limit of the microscope, the spatial random modulation should be performed after the image-encoding part to avoid pattern blurring caused by image-encoding.

To validate the utility of our method, we computationally perform compressed optical time-stretch microscopy with an experimental dataset acquired by a conventional optical time-stretch microscope whose schematic is the same as in Fig. 1 except for the absence of the random mask [12]. In the experimental setup, the pulse laser is a Ti:Sapphire femtosecond laser with a center wavelength, bandwidth, and pulse repetition rate of 780 nm, 40 nm, and 75 MHz, respectively. The groove density of the two diffraction gratings is 1200 lines/mm. The magnification and numerical aperture of the two objective lenses (Olympus) are 40 and 0.6, respectively. The temporal disperser is a 2-km single-mode fiber spool (Nufern) with a group-velocity dispersion of -240 ps/nm. The bandwidth of the photodetector (New Focus) is 12 GHz while the bandwidth and sampling rate of the digitizer (Tektronix DPO 71604B) are 16 GHz and 50 GS/s, respectively. The temporal width of each pulse is 7.4 ns, meaning that, with conventional optical time-stretch microscopy, the maximum repetition rate of the pulse laser (system scanning rate) is 135 MHz to avoid overlapping the consecutive pulses.

The process of compressed optical time-stretch microscopy can be mathematically represented as follows (see Fig. 2). Consider an image with M row pixels and N column pixels we want to obtain. First, a 2-D mask with identical random rows is applied to the sensed image (Step 1). A uniform shift is introduced between each pair of successive rows to model the time delay between the repeated pulses, i.e., the k-th row of the image is shifted by $(k-1)T$ columns (Step 2). Here, T is the number of sampling points during one pulse period. The photodetector makes a measurement by collapsing the image into a 1-D vector by adding up the intensity of each column of the coded, shifted image (Step 3). At low pulse repetition rates, $T > N$ and there is no overlap between successive rows,

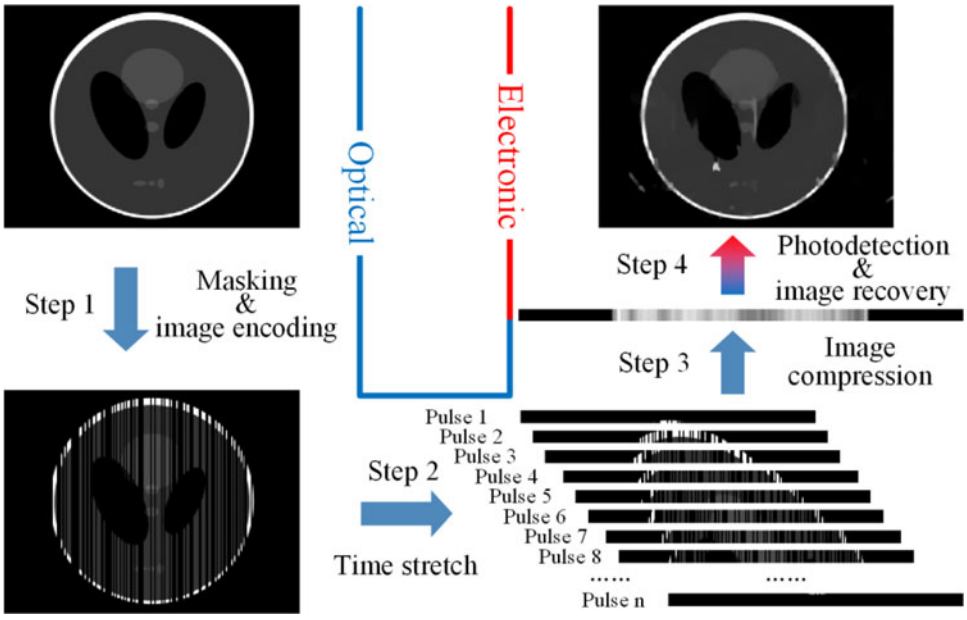

Fig. 2. Principle of compressed optical time-stretch microscopy.

which means that each row of the image can be acquired sequentially. However, at higher pulse repetition rates which applies to our case, $T < N$ and the overlap between the shifted rows leads to fewer measurements than the actual dimensionality of the image. The resulting measurement model is underdetermined. As a consequence, the use of traditional least-squares techniques for recovering the image are often ill-conditioned and riddled with undesirable artifacts. To handle these artifacts and provide robust recovery, we used signal priors to regularize the inverse problem. This is motivated by recent advances in compressive imaging [8]. Specifically, we used the isotropic total-variation norm defined by

$$\rho(I) = \sum_{x,y} \sqrt{[I(x+1,\ y) - I(x,y)]^2 + [I(x,y+1) - I(x,y)]^2} \tag{1}$$

to enforce sparse gradients in the recovered image. The image of the target is recovered by solving the following convex optimization problem (Step 4) given by [8], [9]

$$\hat{I} = \arg\min_I \left\{ E - O(I)^2 + \beta \cdot \rho(I) \right\} \tag{2}$$

where $E \in \mathbb{R}^K$ is the measured signal, $I \in \mathbb{R}^{M \times N}$ is the estimated original image during the iterations ($K < M \times N$), $\hat{I} \in \mathbb{R}^{M \times N}$ is the recovered image, $O: \mathbb{R}^{M \times N} \to \mathbb{R}^K$ is the linear measurement operator which indicates the imaging process, and β is a non-negative scalar that provides a trade-off between data fidelity and gradient sparsity. We used the fast iterative shrinkage-thresholding algorithm (FISTA) [13] to solve the optimization problem. The value of the scalar β was tuned manually. In conventional compressive sensing, the same signal is independently sampled several times with different masks, so that the compression ratio can be conveniently defined as the ratio between the number of the sampling points in the original signal and the number of measurements [8]. However, in our compressed optical time-stretch microscopy, each set of signals is measured only once. For this reason, we define the compression ratio using the overlap ratio of consecutive pulses. Supposing that the overlap ratio of consecutive pulses is given by α ($0 \le \alpha < 1$), the compression ratio can be calculated as

$$\text{Compression ratio} = \frac{M \times N}{N + (M-1)(1-\alpha)N} \approx \frac{1}{1-\alpha}. \tag{3}$$

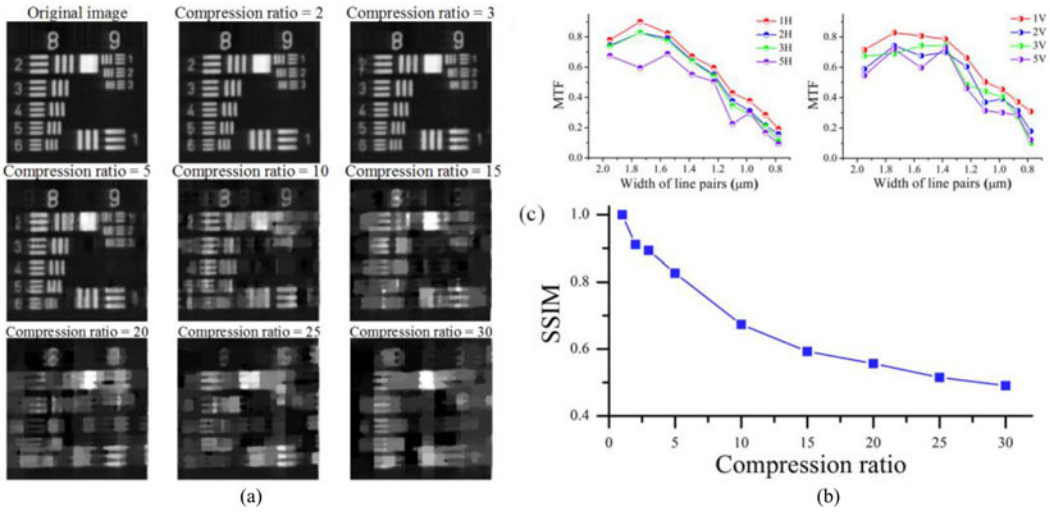

Fig. 3. Demonstration of compressed optical time-stretch microscopy. (a) Images of the USAF-1951 resolution chart at various compression ratios. (b) MTF of the vertical and horizontal line pairs at compression ratios of 1, 2, 3, and 5. (c) SSIM between the original and recovered images at the various compression ratios.

3. Results

The performance of the compressed optical time-stretch microscopy of a standard USAF-1951 resolution chart is shown in Fig. 3(a). Here, as the procedure shows in Fig. 2, we computationally applied the random mask to unmasked images acquired by a conventional optical time-stretch microscope. The finest line pairs of the resolution chart (group 9, element 3) can be clearly distinguished in the original image without the image compression, indicating the resolution of the optical time-stretch microscope is at least higher than 780 nm. As shown in Fig. 3(a), at an increasing compression ratio, the images of the line pairs begin to get blurred with artifacts due to the cross-talk between the pixel rows. To quantitatively evaluate the spatial resolution of the system at different compression ratios, we calculated the MTFs for vertical and horizontal line pairs separately at compression ratios of 1, 2, 3, and 5. Here, the MTF is defined as [10]

$$\mathrm{MTF} = \frac{I_{\max} - I_{\min}}{I_{\max} + I_{\min}} \tag{4}$$

where $I_{\max}$ and $I_{\min}$ are the maximum and minimum intensities in the recovered images for each line pair, respectively. As shown in Fig. 3(b), the MTF of the line pair almost remains the same at compression ratios of less than 3. At the compression ratio of 5, the MTF of the line pair in the group 9 element 3 is still kept at 0.1, meaning that the resolution remains as high as 780 nm while its frame rate is five times higher (i.e., 675 MHz) than that of optical time-stretch microscopy without the image compression (i.e., 135 MHz). Fig. 3(a) and Fig. 3(b) also show that as the compression ratio increases, the microscope's spatial resolution in the horizontal direction (scanning direction) is degraded more quickly than in the vertical direction (moving direction). This is because the image recovery is conducted row by row along the vertical direction, resulting in a relatively low correlation between the pixels in the vertical direction. On the other hand, to quantitatively evaluate the overall imaging performance of the compressed optical time-stretch microscope at different compression ratios, we used the SSIM index, a parameter for evaluating the similarity between two images, defined by [11]

$$\mathrm{SSIM}(x, y) = \frac{(2\mu_x\mu_y + c_1)(2\sigma_{x,y} + c_2)}{(\mu_x^2 + \mu_y^2 + c_1)(\sigma_x^2 + \sigma_y^2 + c_2)} \tag{5}$$

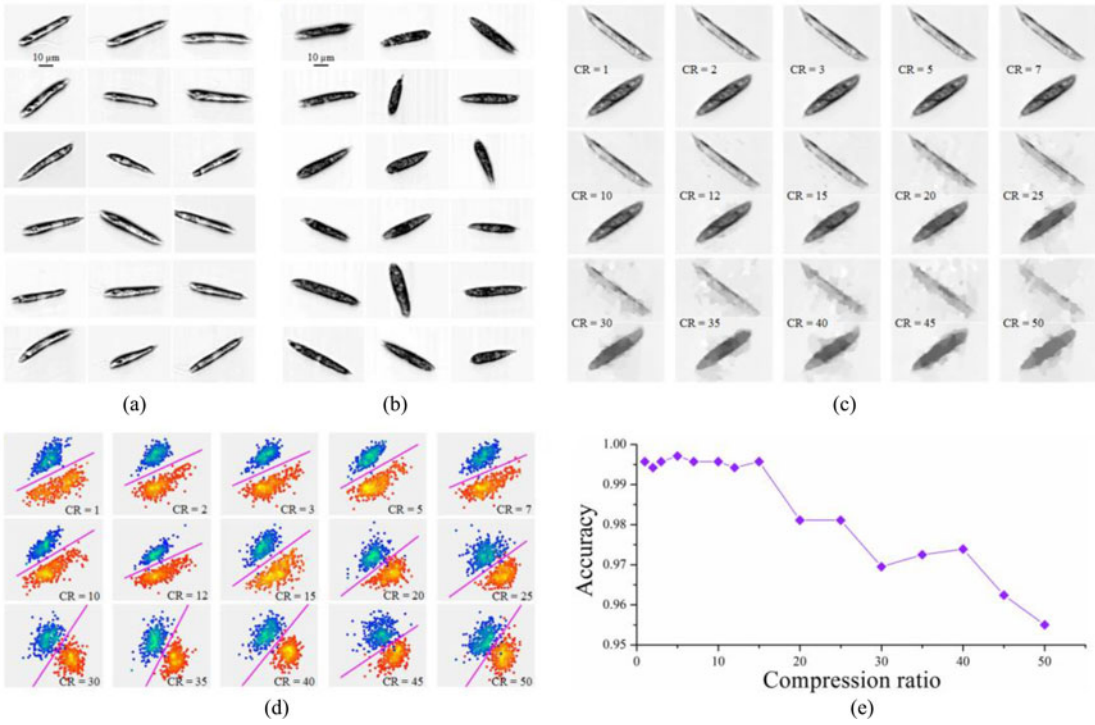

Fig. 4. Cell classification with compressed optical time-stretch microscopy. (a), (b) Image libraries of *E. gracilis* cells without image compression. (c) Recovered images of the fresh and lipid-rich *E. gracilis* cells at various compression ratios. (d) Scatter plots of the fresh and lipid-rich *E. gracilis* cells at the compression ratios. (e) Cell classification accuracy at the compression ratios. CR: compression ratio.

where x and y represent the original and recovered images, respectively; μ_x and μ_y are the average intensity value of the original and recovered images, respectively; σ_x and σ_y are the intensity variance of the original and recovered images, respectively; $\sigma_{x,y}$ is the intensity covariance of the original and recovered images; and c_1 and c_2 are two variables to stabilize the SSIM value. Fig. 3(c) shows the SSIM values at various compression ratios. As expected, the SSIM value decreases as the compression ratio increases, but it still remains higher than 50% even at a compression ratio of 30, indicating a good image recovery performance in our compressed optical time-stretch microscope.

Compressed optical time-stretch microscopy is applicable for high-throughput cell screening without degrading cell screening accuracy. To verify this, we computationally perform compressed optical time-stretch microscopy on the images of a large population of *E. gracilis* cells [14], [15] acquired by a conventional optofluidic time-stretch microscope [12], [16]. *E. gracilis* is known for generating wax esters which can be refined into kerosene for aviation fuels. In our experiments, we cultured *E. gracilis* NIES-48 under two different conditions (nitrogen-sufficient and nitrogen-deficient cultures) to prepare fresh and lipid-induced *E. gracilis* cells [12]. These two different samples were used in the high-throughput cell screening experiments with the conventional optofluidic time-stretch microscope. Furthermore, to acquire cell images without out-of-focus blurring, we used hydrodynamic focusing to align the cells flowing through the microchannel. The details of the microfluidic device are available in our prior paper [12].

Our results are shown in Fig. 4(a) through Fig. 4(e). First, Fig. 4(a) and Fig. 4(b) show the unmasked images of fresh and lipid-rich *E. gracilis* cells taken at a high throughput of 10,000 cells/s without image compression. Nitrogen-sufficient cells with a low lipid content look mostly transparent while nitrogen-deficient cells with a high concentration of intracellular lipids look mostly opaque throughout their entire cell body due to the high concentration of strong intracellular scatterers (presumably accumulated lipid droplets and paramylon particles). Fig. 4(c) shows the recovered images

of the fresh and lipid-rich *E. gracilis* cells at various compression ratios. The figure indicates the gradual degradation of their image quality. The texture of the cells remains visible at a compression ratio of less than 20 while the texture is difficult to recognize with bare eyes at a higher compression ratio of more than 20. After applying cell classification based on support vector machines to the features extracted from the images, such as cell area, aspect ratio, and opacity, each cell can be represented by a single point in a 2-D space expanded by two meta-features for classification. Fig. 4(d) shows scatter plots of these cells at the compression ratios corresponding to Fig. 4(c). The figure shows that the two distinct distributions of the cells merge at large compression ratios, making their separation (hence, the cell classification) unclear. Finally, Fig. 4(e) shows the cell classification accuracy at the compression ratios defined by [17]

$$\text{Accuracy} = \frac{\sum \text{True positive event} + \sum \text{True negative event}}{\text{Total population}}. \tag{6}$$

As the figure shows, the accuracy is kept above 99% at compression ratios up to 15, but starts to degrade at a compression ratio of more than 15. Yet, the accuracy is higher than 95% even at a compression ratio as large as 50 (meaning a line scan rate of 6.75 GHz). This indicates that, by virtue of the image compression, the throughput can be increased up to at least 500 000 cells/s without significantly sacrificing the cell classification accuracy.

4. Discussion

Using images acquired by a conventional optical time-stretch microscope, we theoretically simulated the capability of compressed optical time-stretch microscopy to acquire images with high quality in terms of spatial resolution and accuracy of image-based cell classification at an extremely high frame rate. Although more work needs to be done for practical applications, the work presented here is entirely different from previous work [18], [19] in which optical pulses encoded with the target's information are firstly temporally stretched, modulated with different random masks, and temporally compressed into single pulses for detection, aiming at data-volume reduction at the cost of the scanning rate. In contrast to this, in our work, the pulses encoded with the target's information are firstly spatially modulated with the same random mask, temporally stretched to introduce an overlap between neighboring pulses which is intentionally circumvented in their work, and directly detected without temporal compression, aiming to increase the scanning rate. Our method holds great potential for imaging of fast dynamical phenomena or fast-moving objects.

Acknowledgement

The fabrication of the microfluidic device was conducted at the Center for Nano Lithography and Analysis, University of Tokyo, supported by the MEXT, Japan.

References

[1] G. J. Tearney *et al.*, "In vivo endoscopic optical biopsy with optical coherence tomography," *Science*, vol. 276, no. 5321, pp. 2037–2039, 1997.
[2] S. W. Hell, "Microscopy and its focal switch," *Nature Methods*, vol. 6, no. 1, pp. 24–32, 2009.
[3] A. Greenbaum *et al.*, "Imaging without lenses: Achievements and remaining challenges of wide-field on-chip microscopy," *Nature Methods*, vol. 9, no. 9, pp. 889–895, 2012.
[4] K. Goda, K. K. Tsia, and B. Jalali, "Serial time-encoded amplified imaging for real-time observation of fast dynamic phenomena," *Nature*, vol. 458, no. 7242, pp. 1145–1149, 2009.
[5] K. Goda and B. Jalali, "Dispersive Fourier transformation for fast continuous single-shot measurements," *Nature Photonics*, vol. 7, no. 2, pp. 102–112, 2013.
[6] C. Lei, B. Guo, Z. Cheng, and K. Goda, "Optical time-stretch imaging: Principles and applications," *Appl. Phys. Rev.*, vol. 3, no. 1, 2016, Art. no. 011102.
[7] A. K. Lau, H. C. Shum, K. K. Wong, and K. K. Tsia, "Optofluidic time-stretch imaging—An emerging tool for high-throughput imaging flow cytometry," *Lab Chip*, vol. 16, no. 10, pp. 1743–56, 2016.
[8] J. Romberg, "Imaging via compressive sampling," *IEEE Signal Process. Mag.*, vol. 25, no. 2, pp. 14–20, Mar. 2008.

[9] L. Gao, J. Liang, C. Li, and L. V. Wang, "Single-shot compressed ultrafast photography at one hundred billion frames per second," *Nature*, vol. 516, no. 7529, pp. 74–77, 2014.
[10] H. Fujita *et al.*, "A simple method for determining the modulation transfer-function in digital radiography," *IEEE Trans. Med. Imaging*, vol. 11, no. 1, pp. 34–39, 1992.
[11] Z. Wang, A. C. Bovik, H. R. Sheikh, and E. P. Simoncelli, "Image quality assessment: From error visibility to structural similarity," *IEEE Trans. Image Process.*, vol. 13, no. 4, pp. 600–612, Apr. 2004.
[12] C. Lei *et al.*, "High-throughput label-free image cytometry and image-based classification of live *Euglena gracilis*," *Biomed. Opt. Exp.*, vol. 7, no. 7, pp. 2703–2708, 2016.
[13] A. Beck and M. Teboulle, "A fast iterative shrinkage-thresholding algorithm for linear inverse problems," *SIAM J. Imaging Sci.*, vol. 2, no. 1, pp. 183–202, 2009.
[14] L. Barsanti, R. Vismara, V. Passarelli, and P. Gualtieri, "Paramylon (beta-1,3-glucan) content in wild type and WZSL mutant of Euglena gracilis. Effects of growth conditions," *J. Appl. Phycol.*, vol. 13, no. 1, pp. 59–65, 2001.
[15] R. Danilov and N. G. A. Ekelund, "Influence of waste water from the paper industry and UV-B radiation on the photosynthetic efficiency of Euglena gracilis," *J. Appl. Phycol.*, vol. 11, no. 2, pp. 157–163, 1999.
[16] B. Guo, C. Lei, T. Ito, Y. Jiang, Y. Ozeki, and K. Goda, "High-throughput accurate single-cell screening of *Euglena gracilis* with fluorescence-assisted optofluidic time-stretch microscopy," *PLoS One*, vol. 11, no. 11, 2016, Art. no. e0166214.
[17] T. Fawcett, "An introduction to ROC analysis," *Pattern Recognit. Lett.*, vol. 27, no. 8, pp. 861–874, 2006.
[18] Q. Guo, H. W. Chen, Z. L. Weng, M. H. Chen, S. G. Yang, and S. Z. Xie, "Compressive sensing based high-speed time-stretch optical microscopy for two-dimensional image acquisition," *Opt. Exp.*, vol. 23, no. 23, pp. 29639–29646, 2015.
[19] B. T. Bosworth, J. R. Stroud, D. N. Tran, T. D. Tran, S. Chin, and M. A. Foster, "High-speed flow microscopy using compressed sensing with ultrafast laser pulses," *Opt. Exp.*, vol. 23, no. 8, pp. 10521–10532, 2015.